Photo-assisted self-optimizing of charge-carriers transport channel in the recrystallized multi-heterojunction nanofibers for highly efficient photocatalytic H₂ generation

Zhenyi Zhang, Kuichao Liu, Yanan Bao, Bin Dong*

Key Laboratory of New Energy and Rare Earth Resource Utilization of State Ethnic Affairs Commission, School of Physics and Materials Engineering, Dalian Nationalities University, 18 Liaohe West Road, Dalian 116600, PR China

ABSTRACT

Rational arrangement of nanosized semiconductor components in the multi-heterojunction photocatalyst can lead to the formation of a high-speed transport channel for charge-carriers separation and migration, which provides a promising way to achieve excellent photocatalytic efficiency for solar fuels generation. Herein, we develop a photo-assisted self-optimization strategy to re-build the charge-carriers transport channel in the copper species nanocrystals/TiO₂ electrospun nanofibers with the organic hydrogen-carrier molecules as the photo-reactants. As a result of the dynamics difference of the excitons migration during the photocatalytic process, the binary CuO/TiO₂ heterojunction nanofibers are recrystallized to form the quaternary Cu/Cu₂O/CuO/TiO₂ multi-heterojunction nanofibers that exhibits a higher rate constant ($\sim 1.7 \times 10^8 S^{-1}$) for the interfacial electron-transfer than the former nanofibers ($\sim 0.7 \times 10^8 S^{-1}$) due to the improved charge-carriers transport channel. In this way, a 40-fold enhanced H₂ generation rate was observed on the recrystallized nanofibers photocatalyst during the photocatalytic decomposition of formic acid as compared to the pure TiO₂ nanofibers. Our work presents an available paradigm to skillfully use a transient photo-physicochemical process to mildly engineer a high-quality charge-carriers transport channel in the hetero-nanophotocatalyst for realizing an optimal photocatalytic performance.

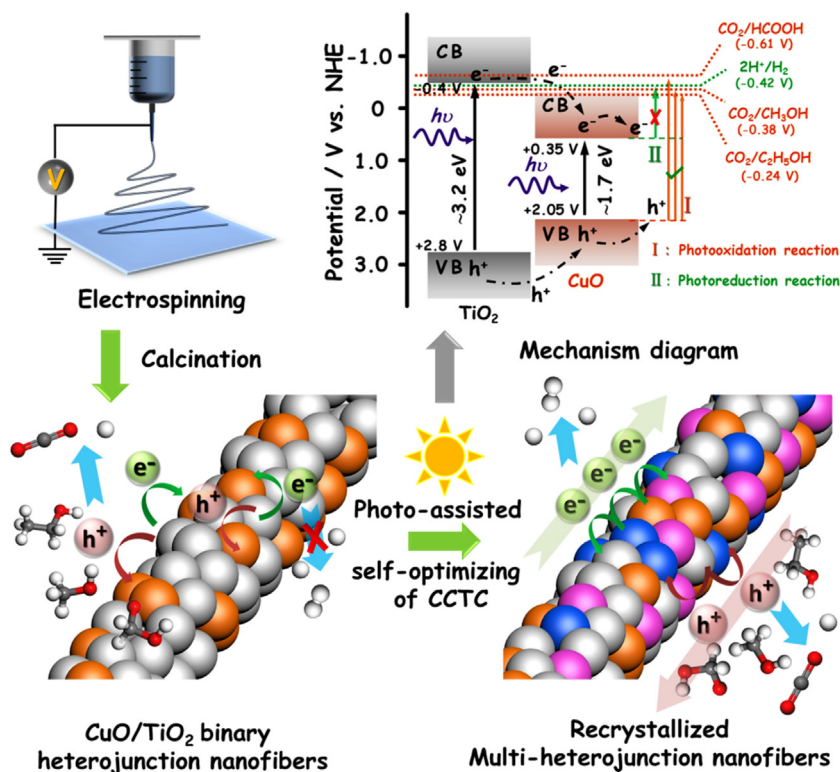© 2016 Elsevier B.V. All rights reserved.

1. Introduction

Engineering the facilitated transport channel for photoinduced charge-carriers separation in a multicomponent nanoscale photocatalyst is a fascinating strategy for maximizing utilization of the absorbed photon energy to fulfill the highly-efficient photocatalytic fuels generation [1,2]. Theoretically, the stepwise energy band structure designed in a nano-heterojunction photocatalyst can result in the formation of an excellent charge-carriers transport channel (CCTC) to effectively guide the photoinduced electrons and holes migration toward the opposite directions for restraining their recombination [3]. However, such CCTC in the artificial heterojunction achieved directly via the physical or wet-chemical synthesis methods often shows a poor efficiency for the exciton dissociation in the photocatalyst body due to a high interfacial "potential barrier" (or discontinuous energy band) at the defec-

tive heterostructural boundary [4]. This drawback seriously hinders high-speed separation and migration of the photoinduced charge-carriers in the photocatalyst. In order to further perfect the CCTC in the heterojunction photocatalyst, the secondary annealing treatment is frequently used for consolidating the hetero-interfacial contact and lowering down the interfacial "potential barrier" [5,6]. Nevertheless, this thermal-improved CCTC in the heterojunction photocatalyst is still unsatisfactory, because a majority of active sites on the photocatalyst surface would be passivated during the secondary annealing process, resulting in the suppressed migration of the separated charge-carriers from the CCTC to the photocatalyst surface for initiating the photocatalytic reaction [7,8]. Thus, it is desirable to build a high-quality CCTC in the well-designed multi-heterojunction photocatalyst without sacrifice of its surface-active-sites. Challenge on achievement of this vision is to seek a moderate synthesis route for the optimal combination of appropriate photoactive components with low hetero-interfacial energy and high active surface.

In this paper, we developed a novel photo-assisted in-situ recrystallization strategy to self-construct an optimal CCTC in the

Scheme 1. Schematic diagrams for the synthesis route of CuO/TiO_2 binary heterojunction nanofibers and the photo-assisted self-optimizing of CCTC through a recrystallization process during the photocatalytic decomposition of organic hydrogen-carrier molecules.

multi-heterojunction photocatalytic system based on the dynamics difference between the photoinduced electrons and holes migration during the photocatalytic decomposition of organic hydrogen-carrier molecules. It is well-known that photocatalytic H_2 generation from the hydrogen-carrier molecules is a two-step overall photoreaction, including the photocatalytic oxidation of the molecule by the photoinduced holes on the valence band (VB) of photocatalyst to produce the H^+, and the photocatalytic reduction of the as-produced H^+ to generate the H_2 by the photoinduced electrons on the conduction band (CB) of photocatalyst [9–11]. Generally, the photocatalytic oxidation reaction should occur before the photocatalytic reduction reaction, because the low oxidation potential of these organic molecules can cause the formation of a deep "potential well", relative to the VB of photocatalyst, to accelerate the photoinduced holes transfer and ensure the release of the stored protons from these molecules (Scheme 1). That is to say, the lifetime of the photoinduced electron may be longer than that of the photoinduced hole at this situation. The long-lived electron with good reducibility would induce a self-reduction process toward the photocatalyst, when the CB of photocatalyst is positioned higher than the redox potential of H^+/H_2 ($\sim$$-0.42$ V). Interestingly, if the crystal structure of the nanoscale semiconductor photocatalyst is dependent on the valence of its composition elements, the above photochemical phenomenon could be employed to dredge the CCTC through the optimal arrangement of energy bands in the recrystallized photocatalyst.

Recently, copper oxides as good hetero-components of the photocatalyst have attracted great attention in the field of photocatalysis research [12–14]. Kum et al. reported an inter-particle charge transfer process between the CuO and TiO_2 nanoparticles, by which simply mixing the TiO_2 and CuO nanoparticles led to a good photocatalytic H_2 production performance [15]. Moreover, Lei et al. proposed a concept of "switching reduction potential by the valence state of copper" in the CuO-modified TiO_2 photocatalytic

system. They found that the CuO could accumulate excess electrons transfer from TiO_2 to form Cu_2O in situ during the induction period, which resulted in an enhanced photo-reductive degradation of 2,2′,4,4′-tetrabromodiphenyl ether [16]. However, the charge-carriers dynamics-induced recrystallization process during the photocatalytic decomposition of hydrogen-carrier molecules is seldom investigated in the CuO/TiO_2 heterostructure, particularly in its one-dimensional nanostructured system.

Herein, we present a successful attempt to self-optimize CCTC in the binary heterojunction photocatalyst of CuO/TiO_2 nanofibers fabricated by a facial electrospinning technique and followed calcination treatment (Scheme 1). After simulated sunlight irradiation for 30 min during the formic acid (HCOOH) photo-decomposition, this binary heterojunction of CuO/TiO_2 changes gradually to a quaternary heterojunction consisting of Cu, Cu_2O, CuO, and TiO_2 nano-components due to the photo-assisted recrystallization reaction caused by the dynamics difference of exciton migration. Accordingly, the CCTC in the heterostructured photocatalyst is adjusted to an optimum condition for promoting the photoinduced charge-carriers separation and migration. As such, the electron-transfer rate constant at the interface between TiO_2 and copper species nanocrystals (Cu, Cu_2O, CuO) reaches $\sim$$1.7 \times 10^8 S^{-1}$, which is $\sim$2.4 times larger than the corresponding value in the CuO/TiO_2 system ($\sim$$0.7 \times 10^8 S^{-1}$), as estimated from the time-resolved transient photoluminescence spectroscopy. Thus, the recrystallized multi-heterojunction nanofibers of $Cu/Cu_2O/CuO/TiO_2$ with a high-quality CCTC exhibit nearly 40-fold enhancement on H_2 generation from the photocatalytic decomposition of HCOOH as compared to pure TiO_2 nanofibers.

2. Results and discussion

TiO_2 and CuO materials are preferentially selected as the heterojunction components to implement the photo-assisted self-

optimizing of CCTC in the nano-heterostructure photocatalyst, since the CB and VB positions of TiO_2 straddle those of CuO to present a "type I" heterojunction interface in which the photoinduced electrons and holes would be accumulated on the CB and VB of CuO, respectively, via a interfacial charge transfer process. As illustrated in Scheme 1, the accumulated holes on the VB of CuO can easily oxidize the HCOOH to produce protons because of their more positive VB potential ($\sim$+2.05 V) as compared to the oxidation potential of CO_2/HCOOH ($\sim$−0.61 V). But, the CB position of CuO ($\sim$+0.35 V) is situated below the reduction potential of H^+/H_2 ($\sim$−0.42 V), which thermodynamically can't drive the photocatalytic reduction of the as-produced protons by the photoinduced electrons. In this way, a recrystallization reaction would occur on the CuO nano-component based on the photo-assisted reduction process. More importantly, the copper species nanocrystals, such as Cu_2O and Cu, may be obtained by photoreducing the CuO component in the CuO/TiO_2 nano-heterojunction, which are the well-known visible-light-active photocatalyst (for Cu_2O), and economic and efficient cocatalyst (for Cu), respectively [17,18]. Moreover, the electrospinning technique enables to align the CuO/TiO_2 bonded nanoparticles along the one-dimensional (1D) direction, which can reduce the depletion zones at the nanoscale heterojunction interface and therefore boost charge transfer from the TiO_2 to the adjacent CuO nanoparticles in the heterojunction nanofibers [19]. Also, the electrospun 1D nanofibrous network structure with high porosity and large surface areas can not only facilitate the light harvesting and charge-carrier migration, but also limit the random diffusion of photo-reduced ions (such as Cu^{2+} or Cu^+) to realize the in-situ self-optimizing of CCTC in the nano-heterojunction photocatalyst through the photo-assisted recrystallization process [20,21].

The crystallographic structure of the as-electrospun binary heterojunction nanofiber is identified as the anatase TiO_2 (JCPDS, no. 21-1272) and tenorite CuO (JCPDS, no. 45-0937) through X-ray diffraction (XRD) analyses (Fig. 1A). The scanning electron microscopy (SEM) and Transmission electron microscopy (TEM) images reveal that the CuO/TiO_2 heterojunction nanofibers aligns in random orientations and have a mean diameter of $\sim$200 nm with lengths up to several micrometers (Fig. 1B and C). Furthermore, the hetero-components of CuO nanocrystals can be distinguishable in the dark-field TEM image, which are dispersed uniformly in the TiO_2 nanofiber matrix. Further observation by the high resolution TEM (HRTEM) image shows the definite nanosized hetero-interface with a relative low lattice mismatch ($(0.35–0.33)/0.35 \approx 5.7\%$) between the $(002)_{CuO}$ plane and the $(101)_{TiO_2}$ plane (Fig. 1D). Meanwhile, the corresponding selected area electron diffraction (SAED) pattern also verifies the co-existence of CuO and TiO_2 nanocrystals to form the heterojunctions in the binary heterojunction nanofibers. Note that a low lattice mismatch means a less defective hetero-interface (or low interfacial "potential barrier"), which is beneficial to charge transfer between the above heterojunction components across the thermal-built CCTC. This hypothesis is well embodied in the X-ray photoelectron spectroscopy (XPS) of CuO/TiO_2 nanofibers. As shown in Fig. 1E and F, the two peaks originated from the binding energy of Ti 2p (458.2 eV for $2p_{3/2}$ and 463.9 eV for $2p_{1/2}$) shifts slightly toward the lower binding energy side as compared to the normal Ti^{4+} ion. Inversely, the characteristic signals of Cu 2p (934.6 eV for $2p_{3/2}$ and 954.8 eV for $2p_{1/2}$) are a little higher than the binding energy of pure CuO reported in the literature [22]. This suggests that a CCTC is built across the interface of CuO/TiO_2 heterojunction to allow the electrons transfer between their Fermi levels. XPS analysis also reveals that the molar ratio of Cu to Ti in the CuO/TiO_2 nanofibers (0.156:1) is very close to the theoretical value (See Supporting information in detail). Moreover, after introducing the narrow bandgap semiconductor of CuO nanocrystals into the TiO_2 nanofiber matrix, the light absorption

behavior of TiO_2 nanofibers is obviously extended from the UV to visible light region (Fig. 1G).

The as-electrospun nanofibrous photocatalysts were then tested for H_2 generation through the photocatalytic decomposition of HCOOH under simulated sunlight irradiation (AM 1.5 with light density of 100 mW cm^{-2}) in Ar atmosphere. Control experiments in the absence of either photocatalysts or light irradiation showed no H_2 generation. As observed in Fig. 2A, the pure TiO_2 nanofibers display a very low H_2 generation rate ($\sim$0.32 μmol h^{-1}) due to their poor light harvesting property, fast recombination of photoinduced charge-carriers, and large overpotential for H_2 generation. And, the visible light absorber of CuO nanofibers does not show appreciable H_2 generation because of its improper CB position related to the H^+/H_2 potential. After coupling CuO with TiO_2 nanoparticles to form the binary heterojunction nanofibers, there was still no H_2 generation under irradiation for 30 min. This observation directly demonstrates the existence of a high-efficient interfacial photoinduced charge transfer from the TiO_2 to CuO via the thermal-built CCTC, leading to the accumulation of photoinduced electrons on the inert CuO surface. To our surprise, when the photo-reaction time was prolonged to 1 h, we observed a remarkable H_2 generation with the rate of $\sim$11.8 μmol h^{-1}, accompanied by the color change of the used photocatalyst from the black-brown to dark-red (inset of Fig. 2A). Then, the photocatalytic H_2 generation rate further increased to $\sim$12.7 μmol h^{-1} after 120 min and became quite stable thereafter. Note that this H_2 generation rate is 39.7 times higher than that of pure TiO_2 nanofibers. Furthermore, the corresponding apparent quantum efficiency (AQE) ($\sim$2.21%) at 365 nm is enhanced 17 times in comparison with the pure TiO_2 nanofibers that only show $\sim$0.13% (See Supporting information). What's more, the photocatalytic H_2-generation activity of the CuO/TiO_2 heterojunction nanofibers is strongly dependent on the molar ratio of Cu to Ti in the nanofibers (Fig. S1). Combination of the above observations, it is reasonable to deduce that the CCTC in the as-electrospun binary heterojunction may be self-optimized through the photo-assisted recrystallization of CuO nanocrystals in the TiO_2 nanofiber matrix.

In the case of photocatalytic decomposition of HCOOH for H_2 generation, the photoinduced holes should be responsible for the oxidation of HCOOH to produce the CO_2 with the molar mass equal to the photoelectrons-reduced H_2 [9]. Thus, to further understand the dynamics difference between the photoinduced electrons and holes migration, the time-dependent CO_2 generation behavior over the CuO/TiO_2 nanofibers was also investigated in comparison with the generated H_2 concurrently. Fig. 2B clearly shows a good linear relation between the generation amount of CO_2 and the irradiation time, implying that the photoinduced holes on the VB of TiO_2 move to the VB of CuO, which then together with the holes exited from the CuO, can implement the photocatalytic oxidation of HCOOH to generate both CO_2 and protons (Scheme 1). However, the similar linear relation appeared on the H_2 generation curve was found after 1 h irradiation. Correspondingly, the molar ratio of H_2/CO_2 increases from 0 at the first 30 min to nearly 0.5 at 1 h, and then approaches to 1 after 2 h. The above results indicate that the stoichiometric decomposition of HCOOH by the photoinduced electrons and holes from the nanofibers photocatalyst is started after simulated sunlight irradiation for 2 h that can be defined as the induction period for the CuO/TiO_2 photocatalyst. It also means that the vast majority of photoinduced electrons are not involved in the photocatalytic decomposition reaction in the induction period, especially, the initial 30 min during which almost all of the photoinduced electrons accumulate on the CB of CuO rather than migrate to the HCOOH molecule. So, the transient migration process between the photoinduced electrons and holes is spatially difference, by which a photo-assisted recrystallization reaction would be expected on the CuO nanocrystals. Note that
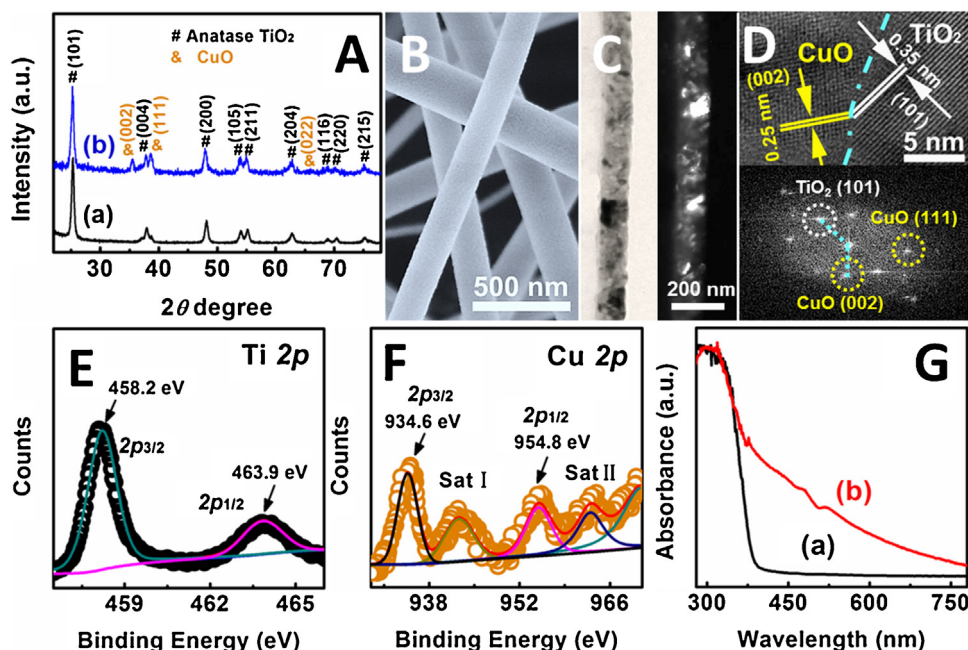
Fig. 1. (A) XRD patterns of the as-electrospun (a) TiO$_2$ nanofibers and (b) CuO/TiO$_2$ heterojunction nanofibers; (B) SEM image, (C) TEM image, and the corresponding dark-field STEM image of the as-electrospun CuO/TiO$_2$ heterojunction nanofibers; (D) HRTEM and the corresponding SAED pattern at the interfacial region of CuO/TiO$_2$ heterojunction; XPS spectrum of (E) Ti 2p core-level and (F) Cu 2p core-level; (G) UV–vis absorption spectra of the as-electrospun (a) TiO$_2$ nanofibers and (b) CuO/TiO$_2$ heterojunction nanofibers.

the gradually increased molar ratio of H$_2$/CO$_2$ during the induction period could be attributed to a slow recrystallization process of CuO nanocrystals in the TiO$_2$ electrospun nanofibers, which implies that the component ratio of Cu, Cu$_2$O, and CuO may be controlled by adjusting the photocatalytic time during the induction period. However, the pure CuO nanofibers did not show an observable recrystallization phenomenon, because its CB potential is too positive to induce the photo-reduction reaction in the CuO nanocrystals. The cyclic voltammograms (CVs) show that, as compared to the CuO/TiO$_2$ binary heterojunction nanofiber that displays only one reduction peak of Cu^{2+} ions around ∼0.61 V, the recrystallized multi-heterojunction nanofiber presents three reduction peaks and one wide oxidation band positioned at ∼0.36 V, ∼0.52 V, ∼0.61 V, and ∼0.36 V, respectively (Fig. 2C), revealing the formation of three kinds of copper species hetero-components after the in-situ photo-reduction of CuO nanocrystals [23–25]. These formed hetero-components would rationally construct an optimal CCTC through the re-arrangement of the energy band configuration in the multi-heterojunction nanofibers for enabling the highly-efficient charge-carriers separation and migration.

This viewpoint can be verified by the incident-photon-to-current-conversion efficiency (IPCE) measurement (Fig. 2D), which reflects to the photoresponse behavior at the different excitation wavelength. Its standard equation can be expressed as:

$$IPCE = \frac{1240I}{\lambda J_{light}} \times 100\%$$

Where λ denotes the incident light wavelength; J_{light} denotes the incident light power density, and I is the photocurrent density [26]. In comparison with the as-electrospun CuO/TiO$_2$ binary heterojunction nanofibers, the recrystallized multi-heterojunction nanofibers exhibit more than twice enhancement in IPCE signal intensity around UV light region, which further confirms the promoted charge-carriers separation and migration after self-optimizing of CCTC based on photo-assisted recrystallization process. Notably, the IPCE response region of the photo-constructed heterojunction nanofibers is extended from the UV light to the

near-infrared light, implying the existence of new visible-light-active absorber. It should be point out that the absorption spectra of CuO/TiO$_2$ nanofibers are inconsistent with their IPCE signal in visible light region. This is ascribed to the unsuitable CB position of CuO that is not capable of reducing the protons even though CuO has a good visible light absorption. The transient photocurrent response tests under several on-off cycles of irradiation reveal stable and high photon-to-electricity efficiency of the recrystallized multi-heterojunction nanofibers in UV light, visible light, as well as near-infrared light region (Fig. 2E). Thus, its H$_2$ generation rate can remain consistent even at the prolonged time period for 12 h (Fig. 2F), which also indicates that when the photo-assisted recrystallization is complete during the photocatalytic HCOOH decomposition, there is a good stability in the recrystallized multi-heterojunction nanofibers.

In order to more clearly identify the crystallographic composition of the recrystallized multi-heterojunction nanofiber, the further systemic structure characterizations were carried out on the nanofibers photocatalyst achieved through natural sedimentation of the CuO/TiO$_2$ nanofibers after 2 h photoreaction. XRD pattern and in-situ TEM diffraction analyses prove the existence of quaternary hetero-components in the recrystallized nanofiber, including the anatase TiO$_2$, tenorite CuO, cuprite Cu$_2$O (JCPDS, no. 05-0667), and cubic Cu (JCPDS, no. 01-1241) (Fig. 3A and Fig. S2). Meanwhile, the recrystallized Cu/Cu$_2$O/CuO/TiO$_2$ nanofibers still remain as long fibrous nanostructure with nearly unchanged diameter compared to the as-electrospun CuO/TiO$_2$ nanofibers (Fig. 3B). As shown in Fig. 3C, the dark-field TEM image indicates that the copper species nanocrystals are more dispersed in the TiO$_2$ nanofiber matrix after the photo-assisted in-situ recrystallization reaction. Furthermore, the lattice fringes and the corresponding SAED patterns, belonging to the $(101)_{TiO_2}$, $(111)_{CuO}$, $(110)_{Cu_2O}$, and $(1\bar{1}0)_{Cu}$ planes, can be easily observed on the HRTEM images of Cu/Cu$_2$O/CuO/TiO$_2$ nanofibers (Fig. 3D). Also, the formation of nanosized hetero-interface regions in the quaternary component nanofibers can promote the charge transfer due to the reduced depletion zones (Fig. S2). The XPS result further confirms that there
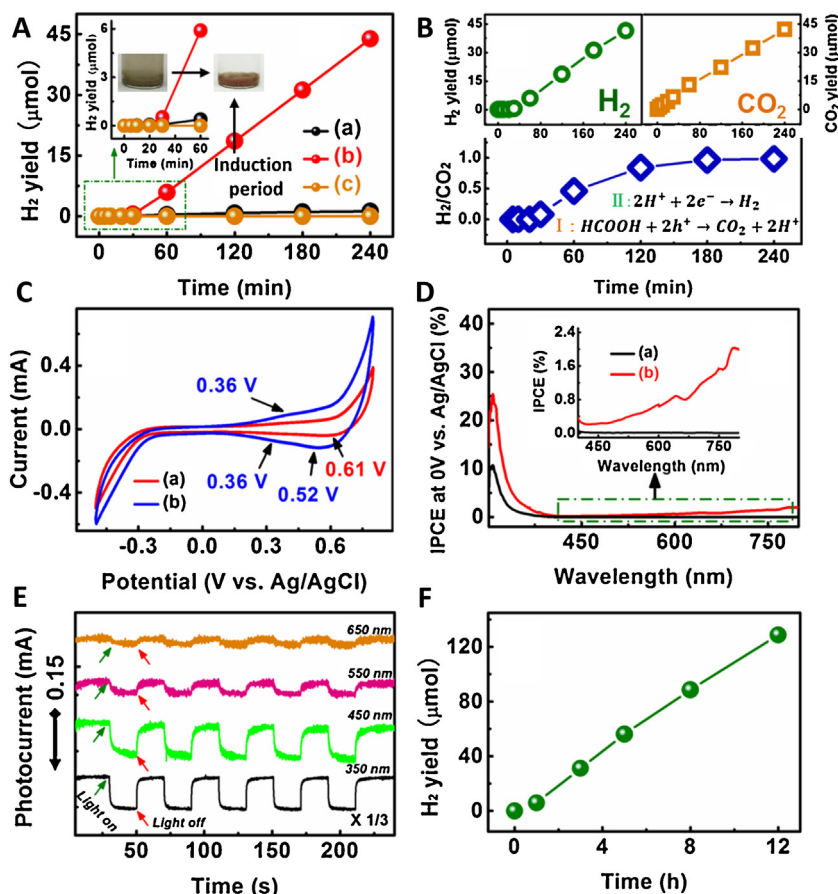
Fig. 2. (A) Time-dependent H_2 generation amount through photocatalytic decomposition of formic acid under AM 1.5 irradiation over (a) TiO_2 nanofibers, (b) CuO/TiO_2 heterojunction nanofibers, and (c) CuO nanofibers; insets are the optical images of the CuO/TiO_2 heterojunction nanofibers before and after the induction period during the photocatalytic reaction, which highlights the color change of the nanofibers photocatalyst; (B) photocatalytic H_2 and CO_2 generation curves over CuO/TiO_2 heterojunction nanofibers in the presence of formic acid under AM 1.5 irradiation, and the corresponding molar ratio of H_2/CO_2 versus irradiation time; (C) CVs of (a) CuO/TiO_2 heterojunction nanofibers and (b) the recrystallized multi-heterojunction nanofibers (meaning the CuO/TiO_2 heterojunction nanofibers after the induction period) in an aqueous solution of 0.1 M NaOH; (D) measured IPCE spectra of (a) CuO/TiO_2 heterojunction nanofibers and (b) the recrystallized multi-heterojunction nanofibers recorded at the incident wavelength range from 300 to 800 nm at a potential of −0.1 V vs. Ag/AgCl in an aqueous solution of 0.1 M NaOH; (E) stable photocurrent test of the recrystallized multi-heterojunction nanofibers under monochromatic light with the wavelength at 350, 450, 550, 650 nm; (F) photocatalytic H_2 generation curve with prolonged irradiation time over CuO/TiO_2 heterojunction nanofibers.

are three valence states for the copper species in the recrystallized nanofibers, for which the peaks with binding energies at 934.2, 955.1, 935.3, 957.2, 936.8, and 958.4 eV are attributed to the Cu^+ $2p_{3/2}$, Cu^+ $2p_{1/2}$, Cu^0 $2p_{3/2}$, Cu^0 $2p_{1/2}$, Cu^{2+} $2p_{3/2}$, and Cu^{2+} $2p_{1/2}$, respectively (Fig. 3E). The binding energies for these peaks are a little different to the normal values, suggesting the existence of charge transfer across the re-built CCTC to equilibrate the Fermi levels in this quaternary heterojunction system [22]. XPS result also reveals that the relative molar ratio of $Cu/Cu_2O/CuO$ is 1:0.94:1.32 in the recrystallized multi-heterojunction nanofibers, which is also the optimal ratio of copper species components for achieving the highly-efficient H_2 generation by photocatalytic decomposition of HCOOH in our case. Moreover, the Cu/Ti molar ratio (0.144) is nearly unchanged in the recrystallized nanofibers (See Supporting information in detail). Accordingly, the light absorption property of the recrystallized nanofiber is obviously promoted (Fig. 3F) and well agreed with the obtained IPCE spectra (Fig. 2D), which powerfully demonstrates that the H_2 generation for the recrystallized nanofiber is induced by the charge-carriers generation due to the light absorption. On the basis of above results and analyses, it is concluded that the inner energy band structure for CuO/TiO_2 heterojunction nanofibers can be re-constructed through the recrystallization of CuO nanocrystals driven by the accumulated photoinduced electrons on their CB during the pho-

tocatalytic decomposition of HCOOH. In this way, the CCTC is also self-modulated to the optimal condition, by which the photoinduced holes on the VB of TiO_2 could transfer to either CuO or Cu_2O for implementing the photocatalytic HCOOH oxidation (Fig. 3G). Meanwhile, the photoinduced electrons would transfer from the CB of Cu_2O to TiO_2 (or directly to Cu surface), then to CuO (or transfer to Cu surface), and finally accumulate on the Cu surface that possesses a stronger binding energy for HCOOH absorption and a lower overpotential for photocatalytic proton reduction [17,18]. It should be point out that in the recrystallized nanofibers, the Cu_2O and CuO components are responsible for harvesting visible light while the TiO_2 component contributes to the UV-light-photocatalytic activity, resulting in a broad photo-responding region of the recrystallized nanofibers. Meanwhile, the metal Cu component, which serves as a low-cost cocatalyst, plays a key role on the collection of the photoinduced electrons to lower down their overpotential for H_2 generation.

The charge-carriers dynamics process in the $Cu/Cu_2O/CuO/TiO_2$ multi-heterojunction nanofibers can be elucidated in detail through time-resolved photoluminescence (TRPL) spectroscopy. The excitation wavelength is selected as 290 nm to induce the interband transitions of all the semiconductor components in the heterojunction nanofibers. It can be found that an obvious decrease in PL intensity occurs when the copper species nanocrys-
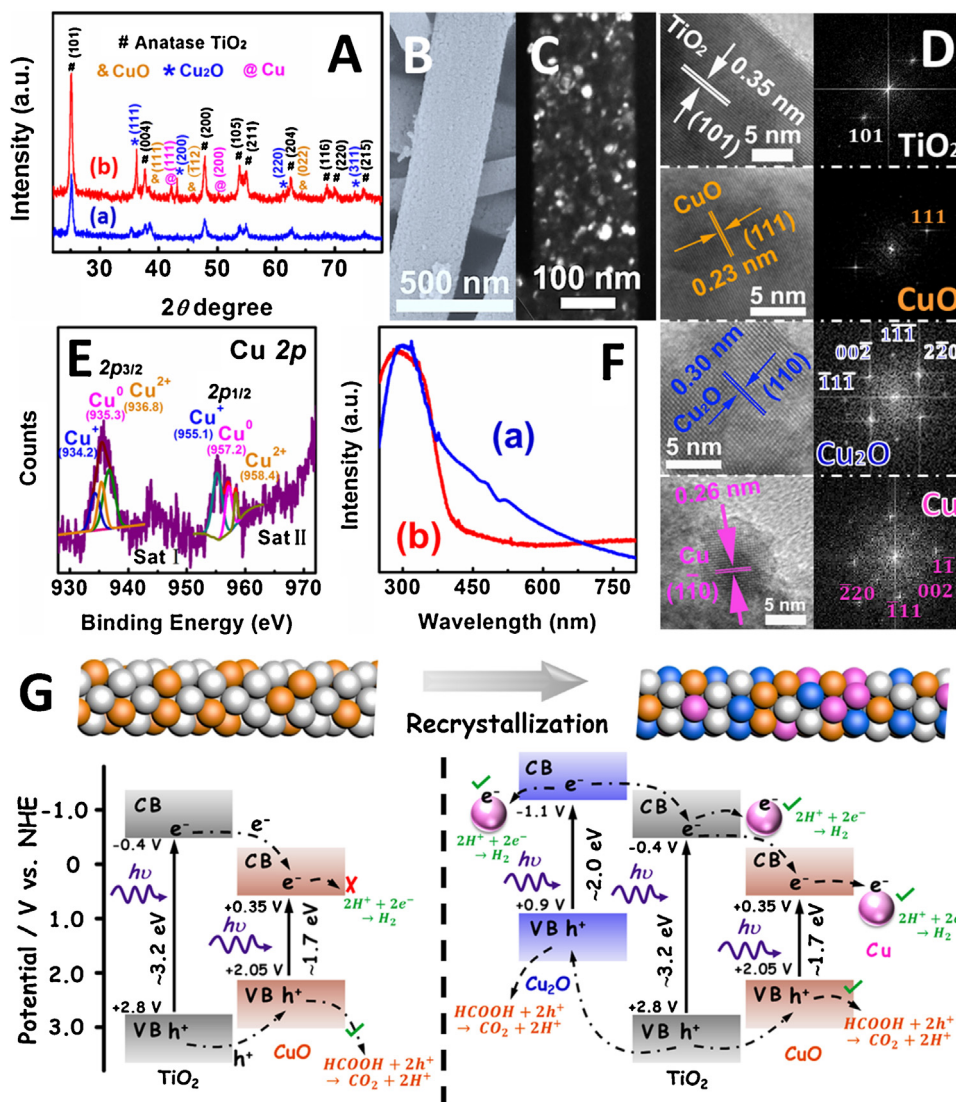
Fig. 3. (A) XRD patterns of the (a) CuO/TiO$_2$ heterojunction and (b) Cu/Cu$_2$O/CuO/TiO$_2$ multi-heterojunction nanofibers; (B) SEM image and (C) dark-field STEM image of the Cu/Cu$_2$O/CuO/TiO$_2$ multi-heterojunction nanofibers; (D) HRTEM and the corresponding SAED pattern of the hetero-components in the Cu/Cu$_2$O/CuO/TiO$_2$ multi-heterojunction nanofibers; (E) XPS spectrum of Cu 2p core-level; (F) UV–vis absorption spectra of the (a) CuO/TiO$_2$ heterojunction and (b) Cu/Cu$_2$O/CuO/TiO$_2$ multi-heterojunction nanofibers; (G) schematic diagram showing the energy band structure transformation and photoinduced charge-carriers transfer in the CCTC before and after the photo-assisted recrystallization process.

tals are introduced into the TiO$_2$ nanofiber matrix (Fig. 4A). In particular, the definable Cu/Cu$_2$O/CuO/TiO$_2$ multi-heterojunction nanofibers show the lowest PL intensity among all the samples. In general, the PL quenching behavior implies either the faster migration with the shorter lifetime or the slower recombination with the longer lifetime of the photoinduced electrons in the heterojunction nanofibers [27]. To further explain this photophysical phenomenon, the TRPL decay signals were fitted by dual-exponential decay kinetics function [28]:

$$I(t) = A_1 \cdot \exp\left(-t/\tau_1\right) + A_2 \cdot \exp\left(-t/\tau_2\right)$$

And, the average emission lifetime, which denotes the overall emission decay behavior of samples, can be also obtained through the following equation:

$$\tau_A = \frac{A_1 \cdot \tau_1^2 + A_2 \cdot \tau_2^2}{A_1 \cdot \tau_1 + A_2 \cdot \tau_2}$$

Where τ_1 and τ_2 are the emission lifetimes, and A_1 and A_2 are the corresponding amplitudes. As listed in the inset of Fig. 4B, the

average emission lifetime of TiO$_2$ nanofibers is decreased from 6.9 to 4.6 ns after coupling TiO$_2$ with CuO nanocrystals. Interestingly, this lifetime further shortens to 3.2 ns for the Cu/Cu$_2$O/CuO/TiO$_2$ nanofibers. The reduced emission lifetime and decreased PL reveal the effective charge-carriers generation and fast electrons migration across the optimal CCTC in the multi-heterojunction nanofibers caused by the emergence of nonradiative quenching pathways [29]. If electron transfer between TiO$_2$ to copper species nanocrystals is the predominant contribution that dictates the emission quenching of TiO$_2$, we can deduce the electron-transfer rate constants (k_{et}) for dynamics process of photoinduced charge-carriers by the following equation [28]:

$$k_{et}\left(CuO/TiO_2 \rightarrow TiO_2\right) = \frac{1}{\langle\tau_A\rangle_{(CuO/TiO_2)}} - \frac{1}{\langle\tau_A\rangle_{(TiO_2)}}$$

$$k_{et}\left(Cu/Cu_2O/CuO/TiO_2 \rightarrow TiO_2\right) = \frac{1}{\langle\tau_A\rangle_{(Cu/Cu_2O/CuO/TiO_2)}} - \frac{1}{\langle\tau_A\rangle_{(TiO_2)}}$$

The results show that the k_{et} in the TiO$_2$/copper species nano-heterojunctions (Cu, Cu$_2$O, CuO) ($\sim 1.7 \times 10^8 S^{-1}$) is ~ 2.4 times
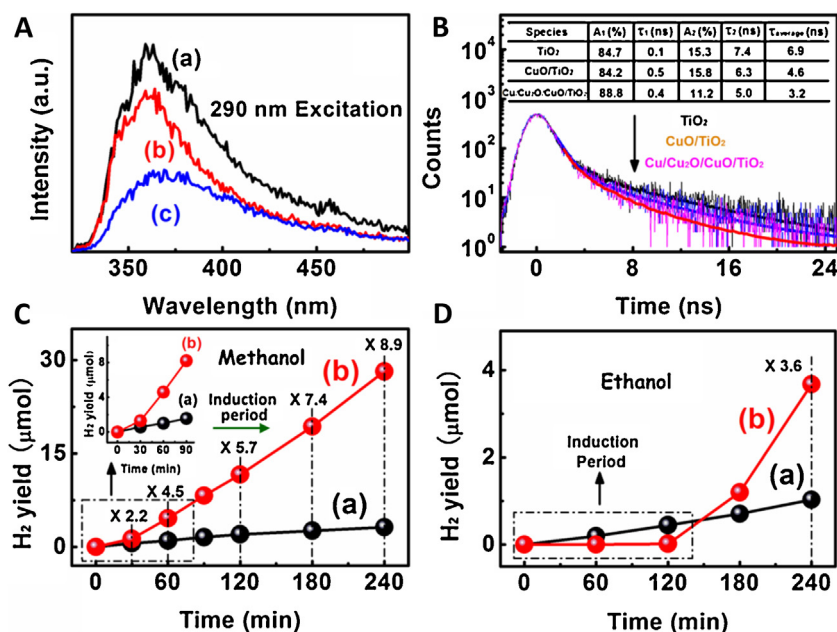
Fig. 4. (A) steady-state PL spectra of (a) TiO$_2$ nanofibers, (b) CuO/TiO$_2$ heterojunction nanofibers and (b) Cu/Cu$_2$O/CuO/TiO$_2$ multi-heterojunction nanofibers; (B) TRPL decay of the nanofibers photocatalysts; time-dependent H$_2$ generation amount through photocatalytic decomposition of (C) methanol and (D) ethanol under AM 1.5 irradiation over (a) TiO$_2$ nanofibers, (b) CuO/TiO$_2$ heterojunction nanofibers which then vary to the copper species nanocrystals/TiO$_2$ multi-heterojunction nanofibers after the induction period.

larger than the corresponding value in TiO$_2$/CuO heterojunction ($\sim 0.7 \times 10^8 S^{-1}$), which provides a solid evidence that a high-quality CCTC is built in the multi-heterojunction nanofibers photocatalyst through a photo-assisted in-situ recrystallization strategy based on the charge-carriers dynamics difference.

To generalize the mechanism of the photo-assisted self-optimizing of CCTC in the CuO/TiO$_2$ heterojunction nanofibers, we employed another two organic hydrogen-carrier molecules (methanol and ethanol) as the photocatalytic reactants to induce the dynamics difference of photoinduced charge-carriers migration because these molecules have the similar oxidation potential to the CO$_2$/HCOOH (Scheme 1). Upon the simulated sunlight irradiation, the H$_2$ generation rates of CuO/TiO$_2$ heterojunction nanofibers are still dependent on the photocatalytic reaction time, as shown in Fig. 4C and D. And, the induction periods for the photocatalytic decomposition of methanol and ethanol are both around 120 min, which suggests that the CCTC in the CuO/TiO$_2$ heterojunction nanofibers is also self-optimized during the induction periods through a photo-assisted in-situ recrystallization process. As such, the optimal H$_2$ generation rates of the recrystallized heterojunction nanofibers are about 8.9 and 3.6 times higher than the corresponding values of pure TiO$_2$ nanofibers for the photocatalytic methanol and ethanol decomposition, respectively. These observations certainly confirm our proposed photo-assisted self-optimizing of CCTC in the heterojunction photocatalyst, which can facilitate the photoinduced charge-carrier separation and accelerate their migration to reach the photocatalyst surface for the highly efficient H$_2$ generation through the photocatalytic decomposition of hydrogen-carrier molecules. The above investigations not only enable us to explicitly understand the photoinduced charge-carriers dynamics process in the nanoscale multi-heterojunction photocatalyst, but also allow us to skillfully use this transient photophysical process to moderately engineer a high-quality CCTC in the appropriate multi-component photocatalytic system for achieving an optimal photocatalytic performance.

3. Conclusions

In summary, we have successfully realized self-engineering high-quality CCTC in the copper species nanocrystals/TiO$_2$ electrospun nanofibers through a photo-assisted in-situ recrystallization process based on the dynamics difference of photoinduced charge-carriers migration. We also demonstrated that, upon simulated sunlight irradiation, the binary heterojunction nanofibers of CuO/TiO$_2$ can transform into the quaternary heterojunction nanofibers of Cu/Cu$_2$O/CuO/TiO$_2$ in the presence of organic hydrogen-carrier molecules as the photo-reactants. Meanwhile, the CCTC in the heterojunction nanofibers is spontaneously polished to an optimum condition for promoting the exciton dissociation and transfer toward the hydrogen-carrier molecules. In the case of photocatalytic decomposition of HCOOH for H$_2$ generation, the photoactivity of the recrystallized Cu/Cu$_2$O/CuO/TiO$_2$ multi-heterojunction nanofibers is nearly 40 times higher than that of pure TiO$_2$ nanofibers. And, its AQE is raised one order of magnitude at 365 nm. Our present work clearly reveals the charge-carriers dynamics behavior in the multi-heterojunction semiconductor photocatalyst during the photocatalytic decomposition of hydrogen-carrier molecules, which offers a facile and effective strategy to develop the low-cost and high-performance semiconductor heterojunction photocatalysts to replace the expensive noble metal-based photocatalysts for application in the solar-to-fuels conversion.

Appendix A. Supplementary data

Supplementary data associated with this article can be found, in the online version, at http://dx.doi.org/10.1016/j.apcatb.2016.10.064.

References

[1] Y. Yuan, L. Ruan, J. Barber, S.C.J. Loo, C. Xue, Energy Environ. Sci. 7 (2014) 3934–3951.
[2] R. Marschall, Adv. Funct. Mater. 24 (2014) 2421–2440.
[3] X. Wang, C. Liow, A. Bisht, X. Liu, T.C. Sum, X. Chen, S. Li, Adv. Mater. 27 (2015) 2207–2214.
[4] F. Wang, A. Dong, W.E. Buhro, Chem. Rev. 116 (18) (2016) 10888–10933, http://dx.doi.org/10.1021/acs.chemrev.5b00701.
[5] R. Wang, L. Gu, J. Zhou, X. Liu, F. Teng, C. Li, Y. Shen, Y. Yuan, Adv. Mater. Interfaces 2 (2015) 1500037.
[6] S. Girish Kumar, K.S.R. Kote swara Rao, Energy Environ. Sci. 7 (2014) 45–102.
[7] C. Yu, G. Li, S. Kumar, K. Yang, R. Jin, Adv. Mater. 26 (2014) 892–898.
[8] J. Cai, Y. Zhu, D. Liu, D. Meng, Z. Hu, Z. Jiang, ACS Catal. 5 (2015) 1708–1716.
[9] S. Kakuta, T. Abe, ACS Appl. Mater. Interfaces 1 (2009) 2707–2710.
[10] K. Shimura, H. Yoshida, Energy Environ. Sci. 4 (2011) 2467–2481.
[11] H. Kisch, Angew. Chem. Int. Ed. 52 (2013) 812–847.
[12] Z. Wang, Y. Liu, D.J. Martin, W. Wang, J. Tang, W. Huang, Phys. Chem. Chem. Phys. 15 (2013) 14956–14960.
[13] A. Paracchino, V. Laporte, K. Sivula, M. Graetzel, E. Thimsen, Nat. Mater. 10 (2011) 456–461.
[14] S.S. Li, H. Bai, Z. Liu, D.D. Sun, Appl. Catal B 140–141 (2013) 68–81.
[15] J.M. Kum, S.H. Yoo, G. Ali, S.O. Cho, Int. J. Hydrogen Energy 38 (2013) 13541–13546.
[16] M. Lei, N. Wang, L. Zhu, Q. Zhou, G. Nie, H. Tang, Appl. Catal B 182 (2016) 414–423.
[17] S. Sun, Nanoscale 7 (2015) 10850–10882.
[18] J.A. Herron, J. Scaranto, P. Ferrin, S. Li, M. Mavrikakis, ACS Catal. 4 (2014) 4434–4445.
[19] D.R. Miller, S.A. Akbar, P.A. Morris, Sens. Actuators B 204 (2014) 250–272.
[20] S.K. Choi, S. Kim, S.K. Lim, H. Park, J. Phys. Chem. C 114 (2010) 16475–16480.
[21] Y. Chen, Y. Chang, J. Huang, I. Chen, C. Kuo, J. Phys. Chem. C 116 (2012) 3857–3865.
[22] J.F. Moulder, W.F. Stickle, P.E. Sobol, K.D. Bomben, Handbook of X-ray Photoelectron Spectroscopy, in: J. Chastain (Ed.), Perkin-Elmer Corp., New York, 1992.
[23] N. Lu, C. Shao, X. Li, T. Shen, M. Zhang, F. Miao, P. Zhang, X. Zhang, K. Wang, Y. Zhang, Y. Liu, RSC Adv. 4 (2014) 31056–31061.
[24] A.J. Bard, J. Jordan, R. Parsons, Standard Potentials in Aqueous Solutions, Marcel Dekker, NewYork, 1985.
[25] Q. Yang, M. Long, L. Tan, Y. Zhang, J. Ouyang, P. Liu, A. Tang, ACS Appl. Mater. Interfaces 7 (2015) 12719–12730.
[26] G. Wang, X. Yang, F. Qian, J.Z. Zhang, Y. Li, Nano Lett. 10 (2010) 1088–1092.
[27] X. Liu, Q. Zhang, J.N. Yip, Q. Xiong, T.C. Sum, Nano Lett. 13 (2013) 5336–5343.
[28] Z. Zhang, Y. Huang, K. Liu, L. Guo, Q. Yuan, B. Dong, Adv. Mater. 27 (2015) 5906–5914.
[29] Z. Bian, T. Tachikawa, W. Kim, W. Choi, T. Majima, J. Phys. Chem. C 116 (2012) 25444–25453.